Supporting Information

Sub-3-nm Rh nanoclusters confined within metal-organic framework for enhanced hydrogen generation

Hui Zhang, [*a] Maolin Huang, [a] Jie Wen, [a] Yanping Li, [a] Airong Li, [a] Lianhong Zhang, [a] Arshid Mahmood Ali, [b] and Yadong Li [c]

[a] The Center of New Energy Materials and Technology, College of Chemistry and Chemical Engineering, Southwest Petroleum University, Chengdu 610500, China

[b] Department of Chemical & Materials Engineering, King Abdulaziz University, Jeddah 72523, Kingdom of Saudi Arabia

[c] Department of Chemistry, Tsinghua University, Beijing 100084, China

E-mail: huizhang@swpu.edu.cn

Table of Contents

1. Experimental Section

Materials

The following chemicals were obtained from Chengdu Cologne Chemical Co. LTD: polyethylene polyvinylpyrrolidone (PVP), sodium borohydride, sodium hydroxide, dimethyl formamide (DMF), methanol, hydrochloric acid (HCl) 37%, zirconium tetrachloride, terephthalic acid, *n*-hexane and ethanol. Rhodium (III) Chloride Hydrate [(RhCl$_3$·nH$_2$O); Rh 38-40 wt%] was obtained from Sigma-Aldrich-China and ammonia borane (H$_3$N·BH$_3$, 97 wt%) was purchased from Aladdin Reagent Co. LTD (Shanghai). Deionized water (DIW) having conductivity of 18.25 Ω was used for all the synthesis. All the chemicals were used without any further purification.

Preparation of Rh nanoparticles (Rh - NPs)

Rh nanoparticles were prepared by using liquid-phase reduction method. 8 mg of RhCl$_3$·nH$_2$O, 2 mg PVP, dissolved in 15 mL of deionized water, were sonicated at 50 °C for 2 hours. Later, 0.030 g NaBH$_4$, dissolved in 5 mL of deionized water was added dropwise in the above solution. The color change from red to black indicated the reduction of Rh^{3+} to Rh-NP$_S$. The solid product obtained after 2 hours of ultrasonic was separated by centrifugation. The obtained sludge was multiple rinsed with ethanol and then vacuum dried at 60 ℃ for 12 hours before using it for further catalyst preparation.

Preparation of UIO-66

0.123 g terephthalic acid, 0.125 g zirconium tetrachloride and 1 mL hydrochloric acid were dissolved in 15 mL DMF by ultrasonic method. The mixture was transferred into stainless steel reactor, lined with polytetrafluoroethylene (PTFE), and was placed in the oven at 120 °C for 24 hours. After the reaction, the reactor was taken out and cooled to room temperature. The white solid product was separated by centrifugation and washed three times by using a solution of DMF and methanol having ratio 4:1. After washing, the final product was dried in vacuum at 120 ℃.

Preparation of Rh/UIO-66 catalyst

Rh/UIO-66 was prepared by using liquid-phase impregnation method. 100 mg of activated UIO-66 dispersed in 30 mL of deionized water, was sonicated for 30 minutes. The freshly prepared Rh − NPs, dissolved in 5 mL of deionized water, was added dropwise to the solution containing UIO-66. It was kept continuously stirred for 5 hours followed by centrifugation. The obtained catalyst was dried under vacuum before using it for catalytic reaction.

Preparation of Rh@UIO-66 catalyst

The metal ion precursor Rh^{3+} was encapsulated into UIO-66 by double-solvent host-guest strategy. In this method, activated UIO-66 (100 mg) was suspended in *n*-hexane (20 mL) as a hydrophobic solvent, and the mixture was sonicated for 30 minutes until it became a homogeneous mixture. After stirring for 2 hours, an aqueous solution of $RhCl_3 \cdot nH_2O$ (30 µL) was added dropwise under vigorous stirring. After continuously stirring for 2 hours, the sludge was filtered, and the powder was dried under vacuum at 100 °C for 12 hours. After dehydration, the Rh ions were reduced to Rh nanoparticles by excess reduction using a newly prepared 0.2 M $NaBH_4$ aqueous solution (3 mL) under intense shaking (220 rpm). The samples were centrifuged and vacuum dried for catalytic reaction.

Catalyst characterization

The X-ray diffraction (XRD) patterns of the samples were measured on an X'Pert PRO MPD diffractometer using a X' Celerator detector and Cu Kα radiation (λ =1.5406 Å) from 5° to 50° with a 2θ step size of 0.02°. Transmission electron microscopy (TEM) images were measured by FEI Titan G2 60-300 field emission transmission electron microscopy. The acceleration voltage was 300 kV. The pore size distribution of the catalyst was measured by N_2 adsorption-desorption at 77 K on Quadrasorb SI analyzer (USA) after 3 hours of degassing at 577 K. Surface area, pore size and pore volume were obtained from N_2 adsorption measurement. Specifically, the pore size DDFT obtained from the maximum value of the pore size distribution curve obtained from DFT method, and the pore volume was calculated from the desorption branch of the N_2 physical adsorption isotherm. The X ray photoelectron spectroscopy (XPS) pattern is measured on Kratos Axis in Britain. The instrument used for ICP-MS is ICP Agilent Technologies 700 Series (ICP-92001).

Ammonia borane(AB) catalytic hydrolysis

The catalytic activity of both Rh/UIO-66 and Rh@UIO-66 the catalysts were determined by measuring the catalytic hydrolysis of AB to hydrogen evolution rate. All the experiments were conducted under same reaction conditions as reported in the literature.[1] In summary, a mixture of catalyst and 5 mL deionized water is added in a three-necked round bottom flask. The flask is placed in a water bath at room temperature and atmospheric pressure. A custom-made tube is connected to the reaction flask to measure hydrogen evolution rate. After this, 30 mg of AB,

dissolved in 200 µL water, was injected into the three-neck round bottom flask by syringe. Hydrogen evolution rate was measured till the end of the reaction. Later, the whole experiment was repeated by using a Rh/AB ratio of 0.0056. After the hydrolysis reaction, the catalyst was recovered by centrifugation. After vacuum drying, the reproducibility tests were conducted under similar reaction conditions as described above.

Alkalinity effect of Rh@UIO-66 catalyst on AB catalytic hydrolysis reaction

The extent of alkalinity effect was studied by using different NaOH concentrations. For this, 0.1 M, 0.2 M, 0.3 M and 0.4 M of NaOH were used. 30 mg AB, dissolved in 200 µL of deionized water, was injected into the three-neck round bottom flask containing a mixture of catalyst and 4 mL deionized water. Hydrogen evolution rate was measured at each alkali concentration under room temperature and atmospheric pressure. The obtained results, with molar ratio of Rh/AB was fixed at 0.0056, are shown in Fig. S13.

2. ICP-MS analysis of Rh@UIO-66 and Rh/UIO-66 catalysts

**Table S1.** Elemental analysis data of catalysts by ICP-MS

Catalysts	Rh loading (wt%) Measured value	Rh loading (wt%) Measured value (four reaction cycles)
Rh@UIO-66	2.83	2.65
Rh/UIO-66	3.01	2.12

The ICP-MS test results showed that the Rh content of Rh@UIO-66 and Rh/UIO-66 catalysts after cycling four times were 2.65% and 2.12%, respectively, compared with 2.83% and 3.01% of the newly prepared catalyst. The decrease in the Rh content of Rh/UIO-66 is more obvious. This indicates that the MOF internal pore of Rh@UIO-66 plays a very good role in limiting the active component, which effectively reduces the loss of Rh nanoparticles during the catalytic process.

3. TEM images of Rh@UIO-66 catalyst
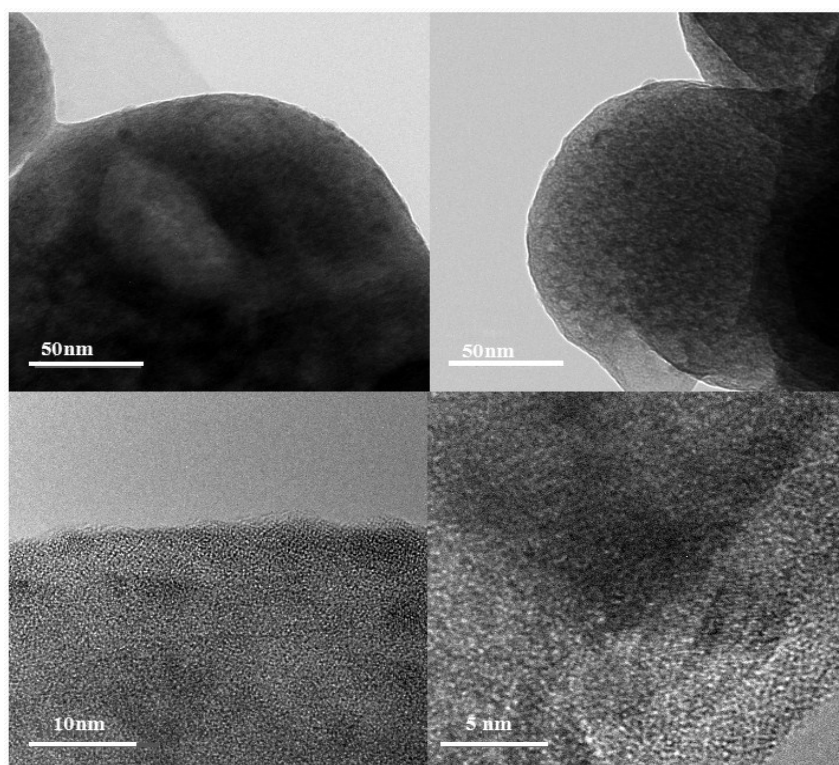
Fig. S1. TEM and HRTEM images of Rh@UIO-66 catalyst.
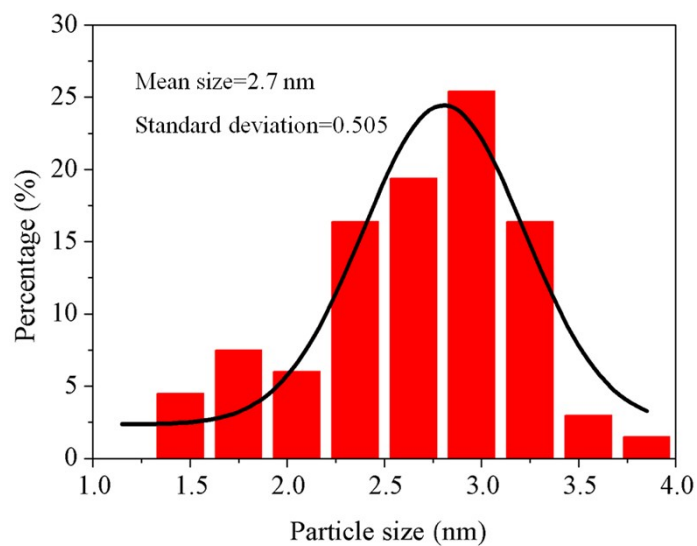
Fig. S2. Size distribution of Rh nanoparticles in Rh@UIO-66 catalyst.
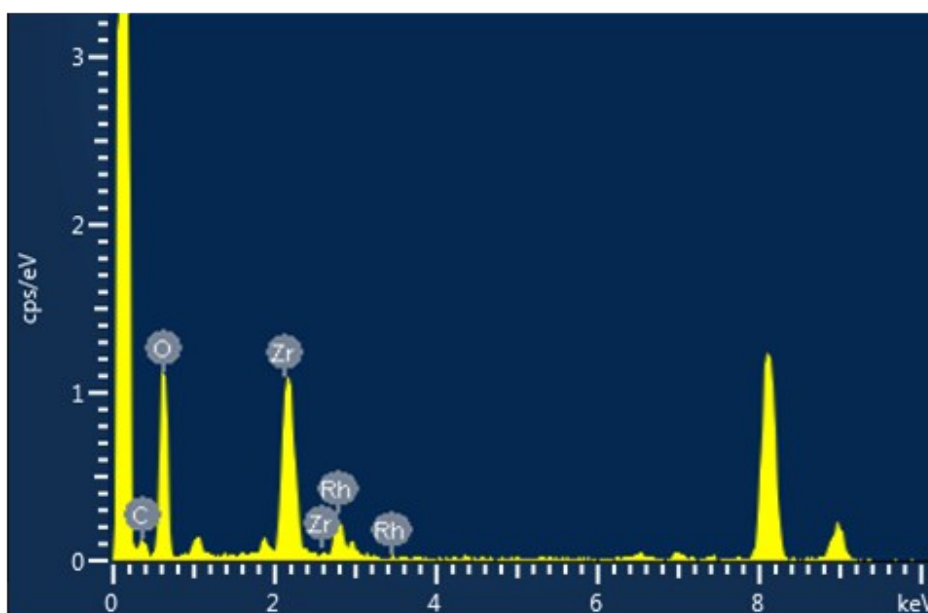
4. EDS image of Rh@UIO-66 catalyst

Fig. S3. EDS image of Rh@UIO-66 catalyst.

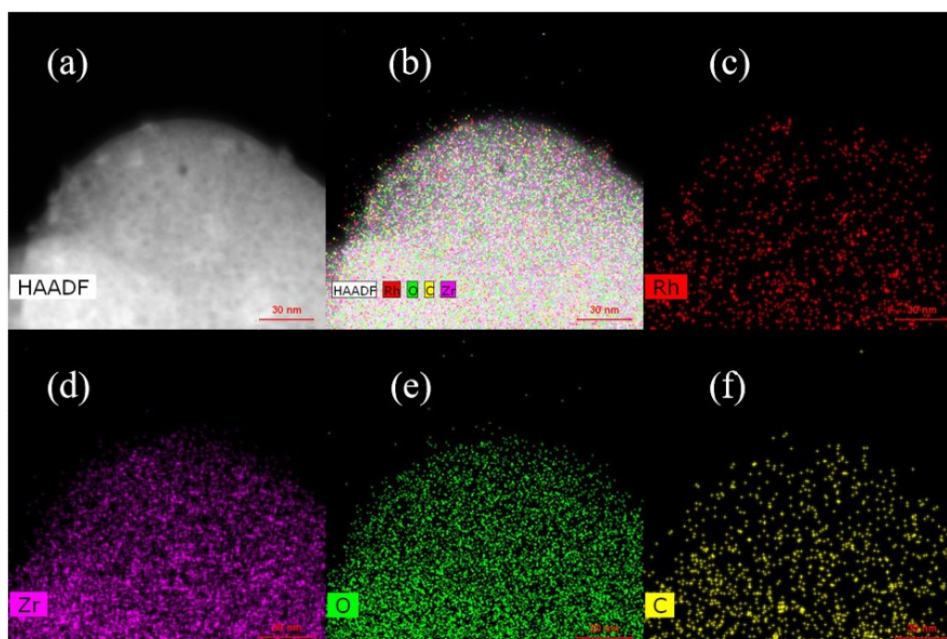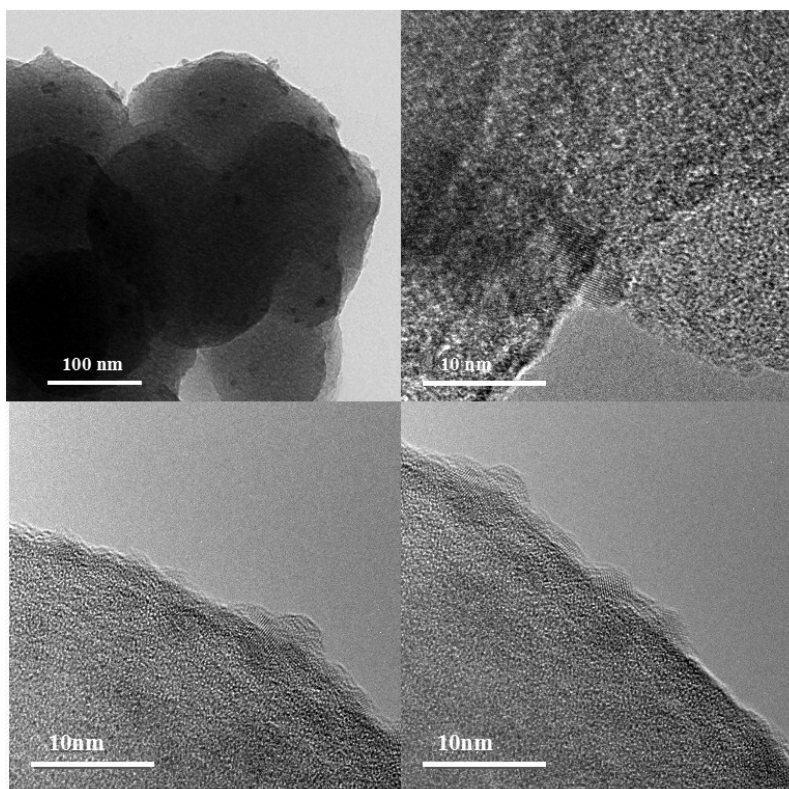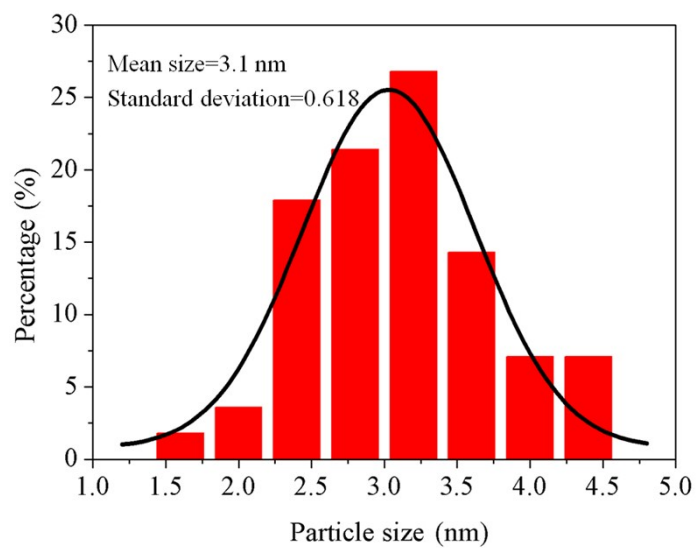## 5. HAADF-STEM and EDX mapping of Rh@UIO-66 catalyst

Fig. S4. (a) HAADF-STEM image of Rh@UIO-66 catalyst and EDX mapping spectra of (b) all element, (c) Rh, (d) Zr, (e) O and (f) C. The scale bar is 30 nm.

6. TEM images of Rh/UIO-66 catalyst

Fig. S5. TEM and HRTEM images of Rh/UIO-66 catalyst.

Fig. S6. Size distribution of Rh nanoparticles in Rh/UIO-66 catalyst.
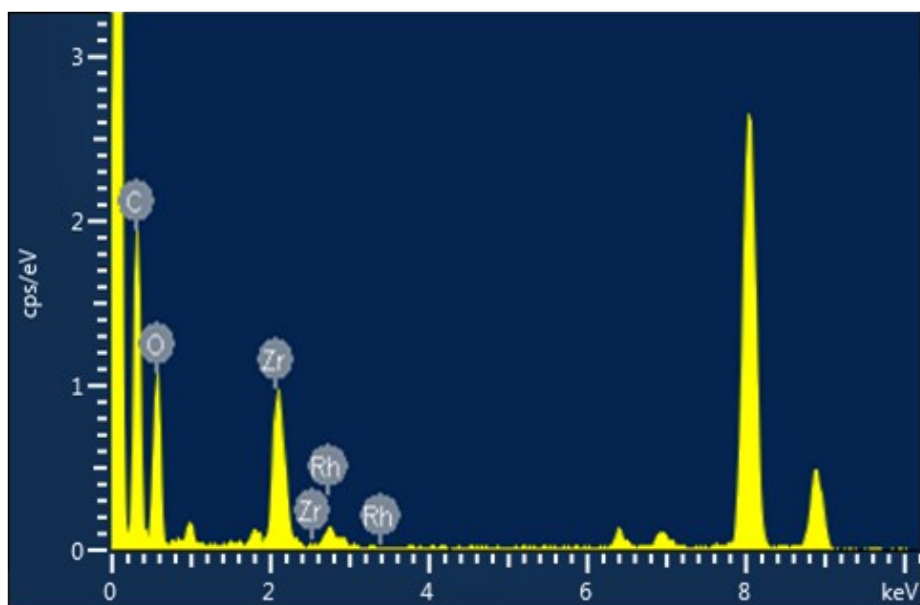
7. EDS image of Rh/UIO-66 catalyst

Fig. S7. EDS image of Rh/UIO-66 catalyst.

8. HAADF-STEM and EDX mapping of Rh/UIO-66 catalyst
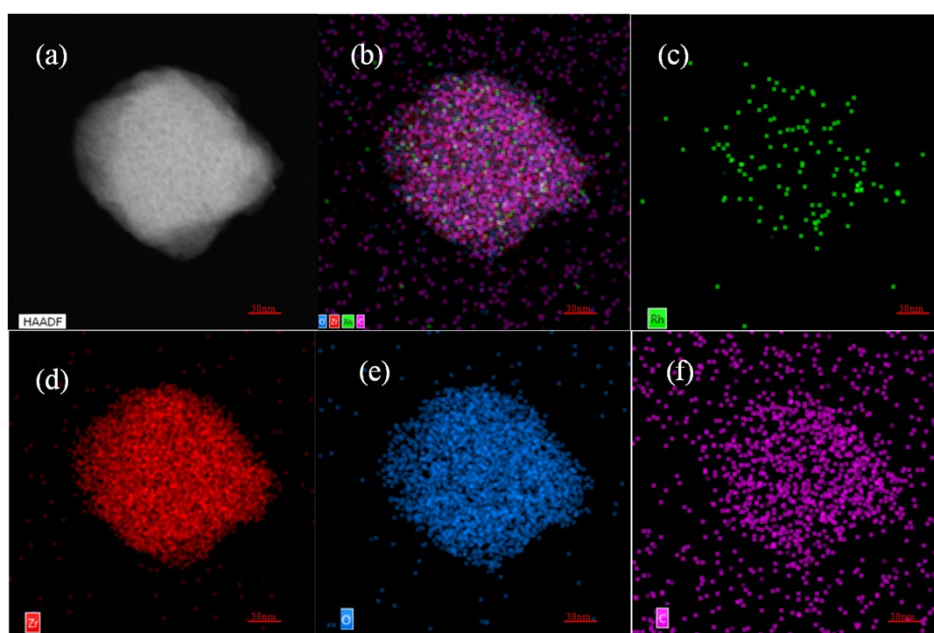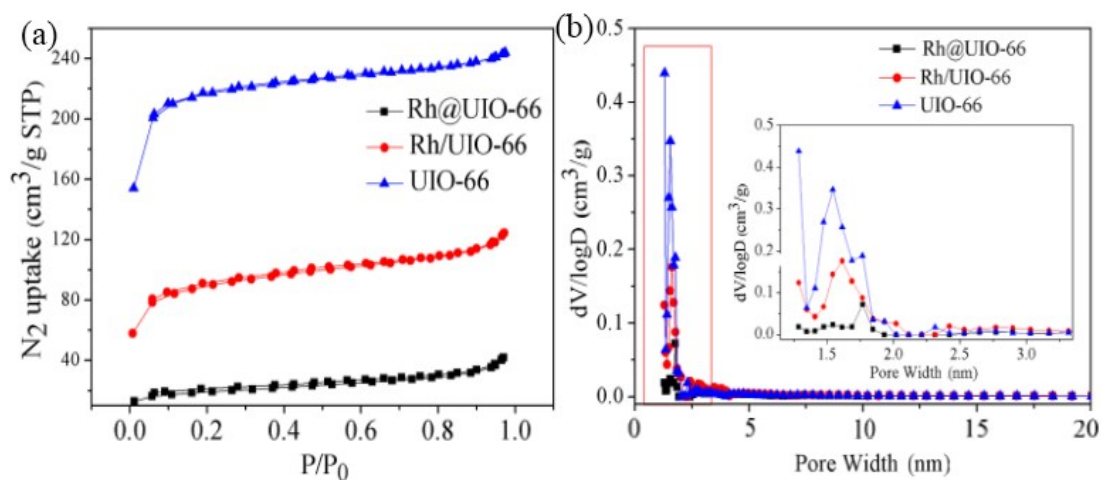

Fig. S8. (a) HAADF-STEM image of Rh/UIO-66 catalyst and EDX mapping

spectra of (b) all element, (c) Rh, (d) Zr, (e) O and (f) C. The scale bar is 30 nm.

9. BET analysis of Rh@UIO-66, Rh/UIO-66 catalysts and UIO-66

Fig. S9. (a) N_2 sorption isotherms of as-synthesized UIO-66, Rh@UIO-66 and Rh/UIO-6 catalysts, (b) pore size distribution of as-synthesized UIO-66, Rh@UIO-66 and Rh/UIO-66 catalysts.

Both the adsorption-desorption isotherms of N_2 on UIO-66 belong to the type-I adsorption-desorption isotherms without hysteresis ring, which is the specific adsorption-desorption isotherms of microporous materials. The adsorption-desorption isotherms of the samples did not change after Rh was introduced into the carrier UIO-66, except the occupation of pore channels by Rh nanoparticles. The BET surface areas and respective pore volumes of UIO-66, Rh/UIO-66, Rh@UIO-66 were 674 m^2/g, 286 m^2/g, 63 m^2/g and 0.377 cm^3/g, 0.192 cm^3/g, 0.0643 cm^3/g respectively.

10. XRD analysis of Rh@UIO-66 ,Rh/UIO-66 catalysts and UIO-66
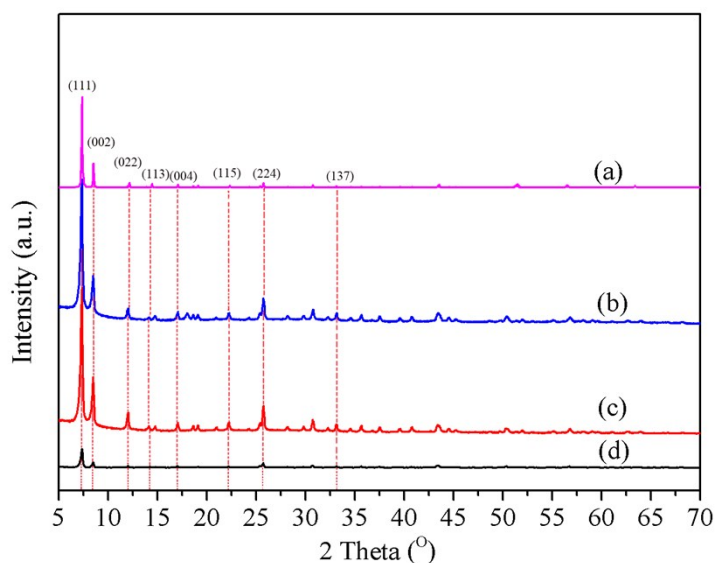
Fig. S10. XRD patterns of (a) simulated UIO-66, (b) as-synthesized UIO-66, (c) Rh/UIO-66 and (d) Rh@UIO-66 catalysts.

The Rh@UIO-66 and Rh/UIO-66 catalysts did not show any loss of crystallinity in the X-ray diffraction pattern after the impregnation and reduction processes, which was similar to the UIO-66. The XRD spectra of UIO-66 show characteristic peaks at 2θ = 7.36°, 8.48°, 12.04°, 14.15°, 17.08°, 22.25°, 25.68°, and 33.12° that correspond to (111), (002), (022), (113), (004), (115), (224), and (137) crystal planes, respectively. It indicates that the integrity of the UIO-66 framework was well maintained. However, the intensity of the diffraction peak of Rh@UIO-66 is weakened to some extent, which may be due to the electrostatic field change caused by the interaction between the electrophilic surface of the nanoparticle and the atom in the host.[2] Further, no diffraction peak of Rh nanoparticles was detected in both Rh@UIO-66 and Rh/UIO-66 catalysts, the loss of XRD diffraction peaks of Rh nanoparticles may be due to the high dispersion of metal nanoparticles and the low loading capacity.[3-5]

11. XPS analysis of Rh@UIO-66 and Rh/UIO-66 catalysts
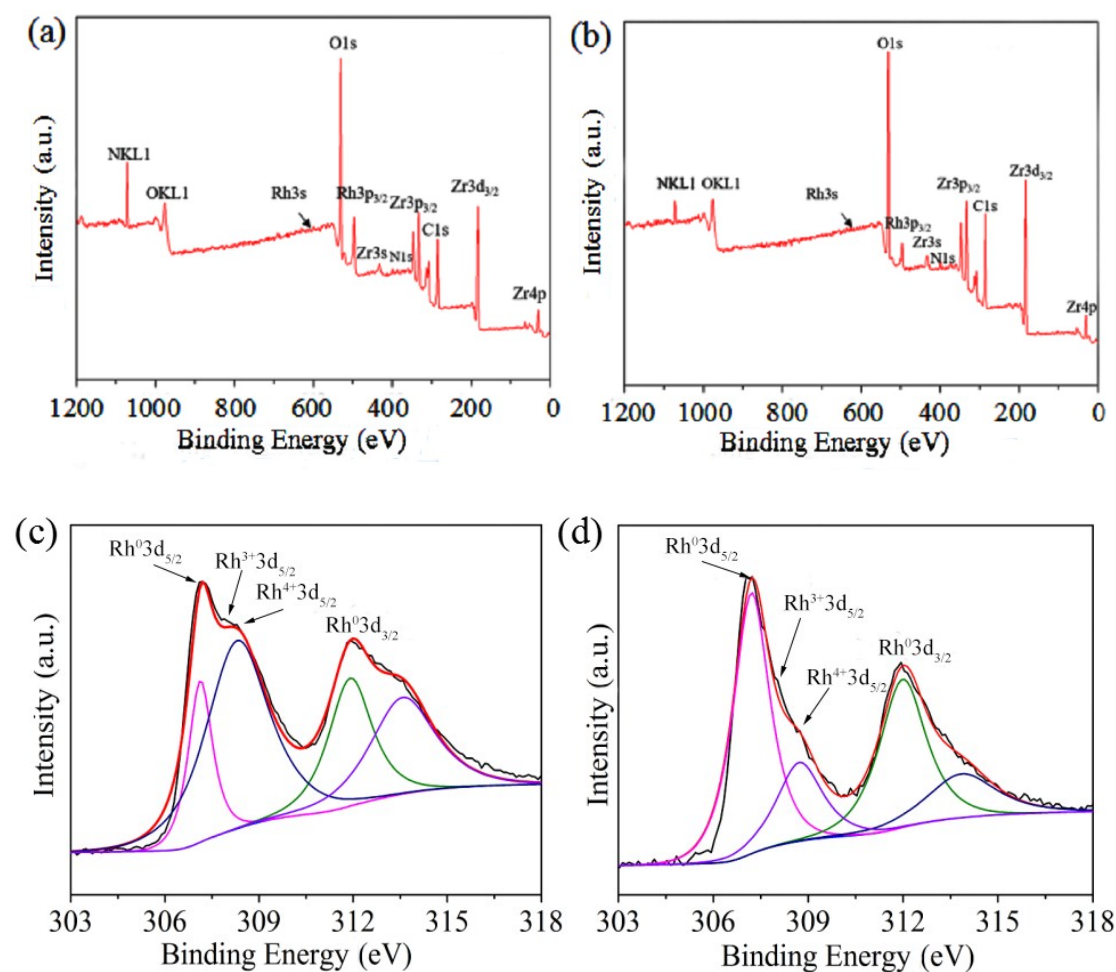
Fig. S11. XPS spectra of (a) Rh@UIO-66 and (b) Rh/UIO-66 catalysts. XPS spectra for Rh $3d_{5/2}$

and $3d_{3/2}$ peaks of (c) Rh@UIO-66 and (d) Rh/UIO-66 catalysts.

The XPS spectrum consists of the Rh $3d_{5/2}$ and Rh $3d_{3/2}$ peaks, produced by spin-orbital splitting. According to the literature,[6-7] the activation energy of Rh $3d_{5/2}$ 307.0 eV - 307.1 eV is attributed to the zero-valent Rh metal. The activation energy of Rh $3d_{5/2}$ orbital in Rh@UIO-66 is 307.2 eV (see Fig. S11 c). The difference of 0.2 eV indicates that the reduced cerium nanoparticles are electron-deficient. At the same time, it was found that there are peaks of Rh $3d_{5/2}$ at 308.3 and 308.6 eV, which correspond to Rh^{3+} and Rh^{4+}, respectively, indicating the presence of Rh_2O_3 and RhO_2. In comparison, the XPS analysis of Rh/UIO-66 showed that the peak of $Rh_{5d3/2}$ at 307 eV corresponds to the zero-valent Rh nanoparticles, and the weak peak of Rh 5d3/2 at 308.3 and 308.6 eV indicates the presence of partial Rh oxides. (see Fig. S11 d).

12. Reusability of Rh/UIO-66 catalyst
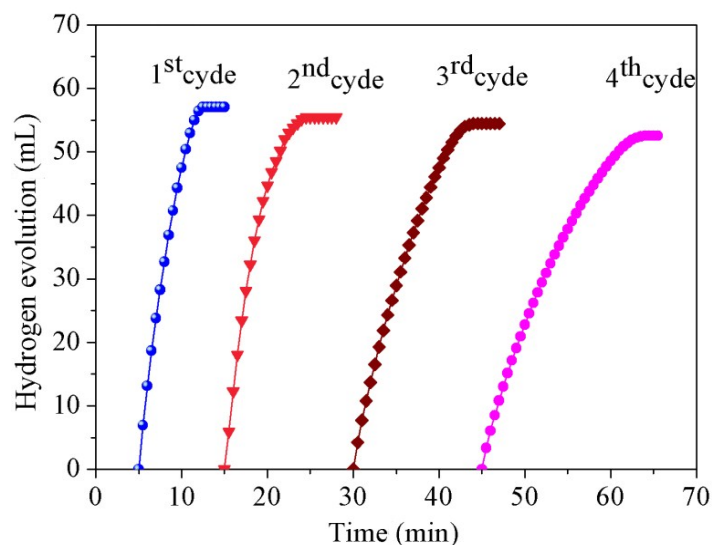
Fig. S12. Reusability of Rh/UIO-66 catalyst.(All tests were carried out at room temperature with a

Rh / AB molar ratio of 0.0056. AB 1.0 mmol).

13. AB hydrolysis test under different NaOH concentration
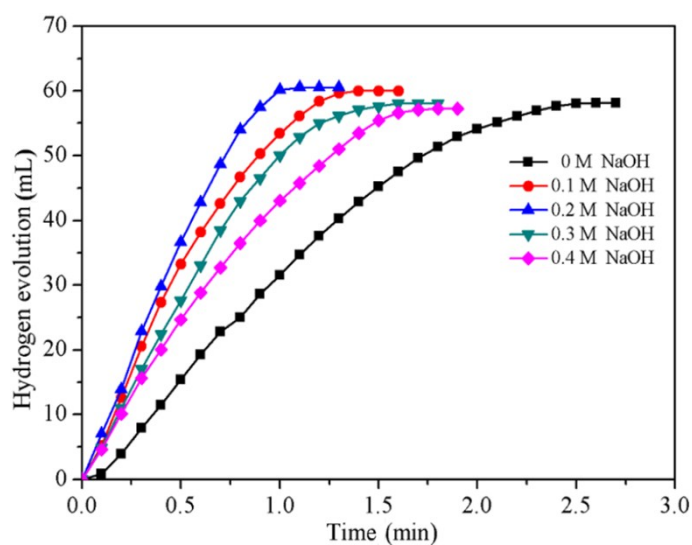
Fig. S13. Hydrogen evolution rate from AB on Rh@UIO-66 catalyst at room temperature with

Rh/AB molar ratio of 0.0056 in the presence of 0 ~ 0.4 M NaOH (for each test, AB 1.0 mmol).

The experimental results showed that the H_2 generation rates firstly increased with the increased in NaOH concentrations (0.1 ~ 0.2 M), and then decreased with higher NaOH concentration (0.3 M). It was observed that the accumulation of excessive OH^-, beyond the optimum level (0.2 M), could significantly reduce the beneficial effect.

14. Activation energy calculation
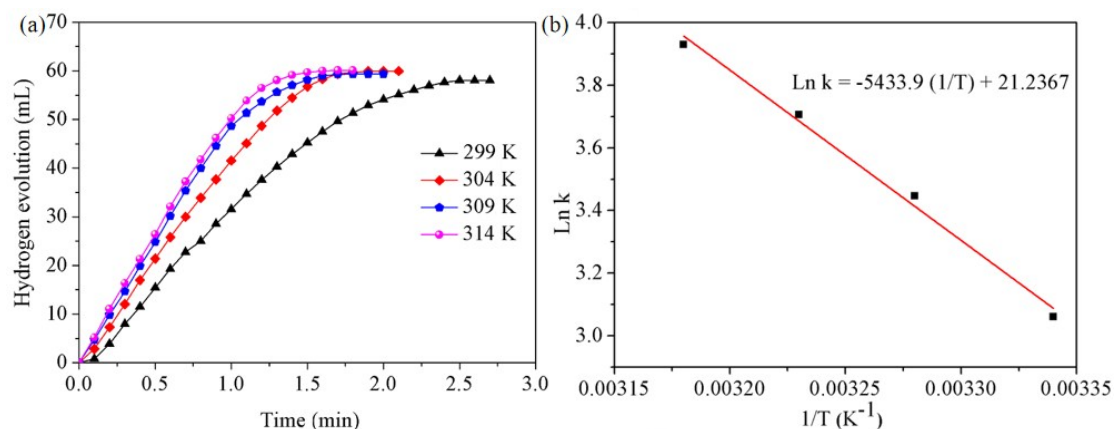
Fig. S14. Hydrogen evolution rate from AB on Rh@UIO-66 catalyst at different reaction temperature with Rh/AB molar ratio of 0.0056 (a), and Arrhenius plots obtained from the kinetic data (b) (for each test, AB 1.0 mmol).

The activation energy (Ea) required for this reaction was 45.2 kJ/mol, calculated by using Arrhenius equation as shown in equation (1)
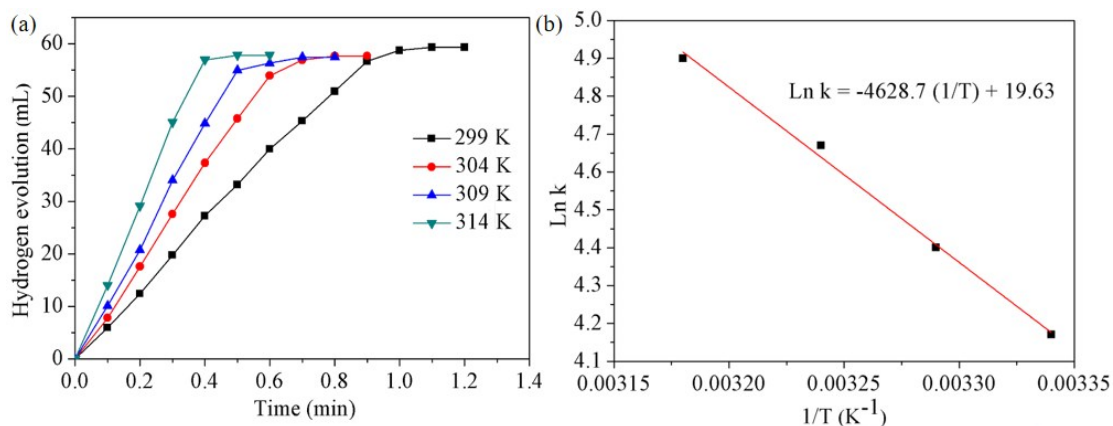
$$\ln k = \ln A - \frac{E_a}{RT} \qquad (1)$$

Where

k : reaction rate;

A : pre-exponential factor;

R : gas constant;

T : reaction temperature.

Fig. S15. Hydrogen evolution rate from AB on Rh@UIO-66 catalyst at different reaction temperature having Rh/AB molar ratio of 0.0056 in the presence of 0.2 M NaOH (a), and

Arrhenius plots obtained from the kinetic data (b) (for each test, AB 1.0 mmol).

The activation energy (Ea) required for this reaction was 38.4 kJ/mol, calculated by equation (1).

15. Turnover frequency (TOF) calculation

$$TOF = \frac{mol_{H2} \text{ released}}{mol_{catalyst} \times \text{reaction time}_{(min)}}$$

where

mol_{H2} released and $mol_{catalyst}$ are the molar amounts of hydrogen produced by a single catalytic reaction and of the metal active component Rh in the catalyst used in the single reaction (calculated according to the ICP-MS test results in table S1); further, the "reaction time" is the time required for a single catalytic reaction.

Table S2. Hydrogen evolution from NH_3BH_3 by Rh@UIO-66 catalyst in different temperatures

Sample	Temperature(°C)	TOF ($mol_{H2} \cdot mol_{cat}^{-1} \cdot min^{-1}$)
Rh@UIO-66	25	219.8
Rh@UIO-66	30	296
Rh@UIO-66	35	330.9
Rh@UIO-66	40	382.3

Table S3. Hydrogen evolution from NH_3BH_3 by Rh@UIO-66 catalyst in the presence of 0 ~ 0.4 M NaOH

Sample	NaOH addition	Temperature(°C)	TOF ($mol_{H2} \cdot mol_{cat}^{-1} \cdot min^{-1}$)
Rh@UIO-66	0 M	25	219.8
Rh@UIO-66	0.1 M	25	414.8
Rh@UIO-66	0.2 M	25	490.6
Rh@UIO-66	0.3 M	25	350.8
Rh@UIO-66	0.4 M	25	300.3

Table S4. Hydrogen evolution from NH_3BH_3 by Rh@UIO-66 catalyst in different temperatures at 0.2 M NaOH

Sample	NaOH addition	Temperature (℃)	TOF ($mol_{H2} \cdot mol_{cat}^{-1} \cdot min^{-1}$)
Rh@UIO-66	0.2 M	25	470.1
Rh@UIO-66	0.2 M	30	608
Rh@UIO-66	0.2 M	35	705.6
Rh@UIO-66	0.2 M	40	813.4

Table S5. Comparisons of literature results on various metal-based nanocatalysts for the hydrolysis of AB. TOF values were given for the hydrolysis of AB at room temperature.

Catalyst	Catalyst/AB (molar ratio)	TOF ($mol_{H2} \cdot mol_{cat}^{-1} \cdot min^{-1}$)	Activation energy, Ea (kJ/mol)	Reference
Rh@UIO-66	0.0056	490.6	38.4	This work
Rh/graphene	0.004	325	19.7	8
Rh^0@TiO_2	0.00116	260	65.5	9
Rh^0/Al_2O_3	0.008	195	---	10
Ru/TiO_2	0.001	604	37.7	11
Ru^0/CeO_2	0.00095	361	51	12
Ru^0/MWCNT	0.00094	329	33	13
Ru@MIL-101	0.008	178	51	14
Pt@MIL-101	0.0029	414	40.7	15
Pt/ -Al_2O_3	0.018	222	---	16
Pd/MIL-101	0.0189	45	---	17
Pd^0/$CoFe_2O_4$	0.0014	290	42	18
Ni^0/$CoFe_2O_4$	0.017	38.3	62.7	19
Ni/CNT	---	23.53	---	20
Ni/SiO_2	0.0225	13.2	34	21

16.   References

1 Z.X. Cai, X.H. Song, Y.R. Wang and X. *Chen, Chemelectrochem*, 2016, **2**, 1665-1671.

2 S. Ding, Q. Yan, H. Jiang, Z. Zhong, R. Chen and W. Xing, *Chem. Eng. J.*, 2016, **296**, 146-153.

3 K. J. Lee, P. A. Kumar, M. S. Maqbool, K. N. Rao, K. H. Song and H. P. Ha, *Applied Catalysis B Environmental,* 2013, **142−143**, 705−717.

4 M. A. Alotaibi, E. F. Kozhevnikova and I. V. Kozhevnikov. *Appl. Catal. A-Gen.*, 2012, **447−448**, 32−40.

5 B. Steinhauer, M. R. Kasireddy, J. Radnik and A. Martin, *Appl. Catal. A-Gen.*, 2009, **366**, 333−341.

6 Y.V. Larichev, O.V. Netskina, O.V. Komova and V.I. Simagina, *Int. J. Hydrogen Energy*, 2010, **35**, 6501-6507.

7 M. Ojeda, M.L. Granados, S. Rojas, P. Terreros, F.J. GarcíA-GarcíA and J.L.G. Fierro, *Appl. Catal. A-Gen.*, 2004, **261**, 47-55.

8 J. Shen, Y. Lan, H. Kai, L. Wei and G. Cheng, *Int. J. Hydrogen Energy*, 2015, **40**, 1062-1070.

9 S. Akbayrak, S. Genç, I. Morkan and S. Özkar, *Rsc. Adv.*, 2014, **4**, 13742-13748.

10 S. Akbayrak, Y. Tonbul and S. Özkar, *Applied Catalysis B Environmental*, 2016, **198**, 162-170.

11 K. Mori, K. Miyawaki and H. Yamashita, *Acs Catal.*, 2016, **6**. 28-35.

12 S. Akbayrak, Y. Tonbul and Ö. S, *Dalton T.*, 2016, **45**, 69-78.

13 S. Akbayrak and S. Ozkar, *Acs. Appl. Mater. Interfaces*, 2012, **4**, 6302-6310.

14 S. Roy, P. Pachfule and Q. Xu, *Eur. J. Inorg. Chem.*, 2016, **27**, 43-53.

15 A. Arshad, K. Abhi, C. Young Joon, T. Nobuko, R. N. Ewa, A. Tom, S. Hiroshi and X. Qiang, *J. Am. Chem. Soc.*, 2012, **134**, 13926-13929.

16 M. Chandra and Q. Xu, *J. Power Sources*, 2007, **168**, 135-142.

17 H. Dai, J. Su, H. Kai, L. Wei and G. Cheng, *Int. J. Hydrogen Energy*, 2014, **39**, 4947-4953.

18 J. Manna, S. Akbayrak and S. Özkar, *Applied Catalysis B Environmental*, 2017, **208**, 104-115.

19 J. Manna, S. Akbayrak and Ã. Z. S, *J. Colloid Interface Sci.*, 2017, **508**, 359-368.

20 G. Zhao, J. Zhong, J. Wang, T. K. Sham, X. Sun and S. T. Lee, *Nanoscale*, 2015, **7**, 9715-9722.

21 M. Onder, M. Vismadeb, O. Saim and S. Shouheng, *J. Am. Chem. Soc.*, 2010, **132**, 1468-1469.